Terahertz spectroscopy of low-energy excitations in charge-ordered $La_{0.25}Ca_{0.75}MnO_3$

T. Zhang,[1] E. Zhukova,[1,2] B. Gorshunov,[1,2] D. Wu,[1] A. S. Prokhorov,[2] V. I. Torgashev,[3] E. G. Maksimov,[4] and M. Dressel[1]
[1]*1. Physikalisches Institut, Universität Stuttgart, Pfaffenwaldring 57, 70550 Stuttgart, Germany*
[2]*A.M. Prokhorov Institute of General Physics, Russian Academy of Sciences, Vavilov Str. 38, 119991 Moscow, Russia*
[3]*Faculty of Physics, Rostov State University, Zorge Str. 5, 344090 Rostov-on-Don, Russia*
[4]*Lebedev Physics Institute, Russian Academy of Sciences, Leninsky Prospect, 53, 119991 Moscow, Russia*
(Received 20 January 2010; revised manuscript received 19 February 2010; published 30 March 2010)

The low-energy electrodynamic response of a series of $La_{0.25}Ca_{0.75}MnO_3$ samples of different morphology is systematically studied in the frequency range from 4 to 700 cm^{-1} (0.1–20 THz, quantum energies 0.4–90 meV) with particular attention focused at frequencies below 40 cm^{-1}. In the antiferromagnetically ordered phase below 140 K, a resonancelike absorption band appears in the spectra around 20–40 cm^{-1} that is assigned to acoustical phonons which acquire optical activity due to a fourfold superstructure appearance in the crystallographic *a* direction and correspondent Brillouin-zone folding. Nanosize effects in charge and magnetic subsystems are investigated by measuring the spectra of samples with grain diameters reduced from several micrometers down to 40 nm. A strong relaxation in the lowest-frequency spectra is observed above 100 K in all samples, indicating that the charge-order transition shows characteristics typical for order-disorder transitions.

DOI: 10.1103/PhysRevB.81.125132 PACS number(s): 75.47.Lx, 73.20.Mf, 71.45.Lr, 75.50.Tt

I. INTRODUCTION

The family of manganese oxides $R_{1-x}A_xMnO_3$ (with *R*, rare earth and *A*, alkaline elements) has originally attracted attention due to the effect of colossal magnetoresistance.[1,2] Eventually it was realized that these compounds are of much broader importance because they represent a diverse playground for investigation of electronic-correlation effects in solids. A unique feature of these materials is the closeness of energies of various types of ground states resulting from comparable strength of different competing interactions and order parameters in magnetic, charge, orbital, and crystal-lattice subsystems.[3–5] This delicate balance makes it possible to tune between various phases by relatively small variations in external and internal parameters—temperature, magnetic and electric fields, pressure, strain, irradiation, and even morphology, such as the granularity with different grain sizes.[6–14] The interplay of different order parameters becomes evident in a rich phase diagram of manganites that contains certain kinds of charge, magnetically and orbitally ordered phases, or even an intrinsically driven mixture of phases (phase separation).[5] The microscopic nature of these states and the mechanisms of corresponding phase transitions are presently far from being completely understood; and this keeps the study of manganites in the focus of today's solid-state physics, also in the broad context of physics of transition-metal oxides including cuprate and noncuprate high-temperature superconductors.

In recent years much effort has been devoted to the intriguing phenomenon of charge ordering (CO) which underlies most effects in overdoped manganites. For the $La_{1-x}Ca_xMnO_3$ (LCMO) the CO transition takes place in the concentration range $0.5 \leq x \leq 0.85$, at rather high temperatures; for instance, at $T_{CO}=250-260$ K in the case of $x=5/8$.[15] Below T_{CO} the magnetic sector of this LCMO system changes its state, from paramagnetic (PM) to antiferromagnetic (AFM). Although it is clear that all degrees of freedom, such as spin, charge, orbital, and phonon, must participate in the charge-ordering process, its detailed mechanism is under intense debate and the experimental results are contradictory. It was believed first that doping of $LaMnO_3$ by Ca leads to dissociation of the mixed-valenced manganese ions into two subsystem with integer valences, Mn^{3+} and Mn^{4+}, which occupy different atomic sites of the lattice[16] and can form spatial stripes composed of Mn^{3+} and of Mn^{4+} for commensurate dopings ($x=\frac{1}{2},\frac{2}{3},\frac{3}{4}$), with periods of integer multiples of the lattice constant in the *a* direction, or bistripes for intermediate dopings,[17–19] composing mixtures of phases with periodicities corresponding to adjacent commensurate dopings. However, this oversimplified picture was called into question[19,20] and it was demonstrated that the spatial charge modulation possesses an amplitude smaller than one and a periodicity with the wave vector q^* that is concentration dependent, $q^*=a^*(1-x)$ (here a^* is the reciprocal-lattice wave vector) and not necessarily tied to atomic sites.[21–24] The situation looks similar to that in $BaBiO_3$ where the "breathing" instability in the lattice was associated with the presence of bismuth ions with the different integer valences, Bi^{3+} and Bi^{5+}, with the Bi^{4+} ions assumed to be unstable. However, as was shown by one of the present authors,[25] there is no dynamic instability of the Bi^{4+} ion and also the breathing instability appears together with the small charge transfer from one Bi ion to another ($Bi^{4+\delta}$-$Bi^{4-\delta}$).

Recently, an idea was put forward[26] that the driving force of the ordering might be of the Peierls-Fröhlich type when the system minimizes its energy due to electron-phonon interaction leading to the formation of a charge-density wave (CDW).[27] Some groups claimed, that the typical prerequisite for the CDW-state occurrence are observed in manganites systems: such as the Fermi-surface nesting,[28] superstructure in the crystal lattice,[23,29] together with the transport signatures of the CDW state, such as the nonlinear dc resistivity and broadband noise.[30,31] Terahertz (THz) and infrared (IR) spectroscopic measurements[32,33] on $Nd_{1-x}Sr_xMnO_3$, $La_{1-x}Ca_xMnO_3$, and $Pr_{1-x}Ca_xMnO_3$ reveal resonances in the far-IR range which are interpreted by the authors as collec-

tive phase modes arising from the CDW condensate. Although the general idea seems intriguing,[34] several important questions arise, and more optical experiments, but also other probes, are needed to unambiguously identify or disprove the CDW state in charge-ordered manganites.[35,36]

Optical spectroscopy has proved to be a powerful experimental technique in studying correlation effects in solids.[37–39] It provides fundamental microscopic characteristics of charge carriers such as concentration, scattering rate, mobility, plasma frequency, effective mass, their temperature, magnetic field, and energy dependences. As for manganites, the majority of optical investigations have been performed in the course of studying the mechanism of colossal magnetoresistance, for example, Refs. 40–42. Besides phonon and polaron bands, these measurements indicate the presence of a charge gap 2Δ in the infrared conductivity spectra in the CO state. The gap disappears under application of magnetic field of several Teslas, when an intense Drude component shows up that is related to metallic conduction. The value of the ratio $2\Delta/T_{CO}$ can be as large as 30 (in LCMO for $x=0.5$) and a pseudogap is seen also above T_{CO} which can be assigned to the CO fluctuations. Only few optical experiments explore the charge-ordered state in the energy range of few millielectron volts where characteristic fingerprints of cooperative charge dynamics typically reveal themselves.[37,38,43]

Our aim was to investigate the charge-ordering phenomena in manganites by examining their electrodynamic response at very low energies down to 0.4 meV. In this paper we present our results obtained for $La_{0.25}Ca_{0.75}MnO_3$. For this composition, upon cooling the compound first undergoes a PM charge-disordered to charge-ordered phase transition at about $T_{CO} \approx 240$ K with coexistence of PM phase and AFM clusters. With further reducing the temperature, the AFM phase evolves around $T_N \approx 140$ K with coexistence of C and CE-type magnetic structure. The CO phase is very stable and insensitive to magnetic fields up to 14 T due to a strong Jahn-Teller distortion and firm AFM structure.[44] Since single crystals of that high Ca concentrations are not available, we have to restrain ourselves to polycrystalline samples. We were, in fact, able to draw advantage out of this constrain, that provided us with extra means to gain insight into magnetic and charge properties of the compound. By varying the samples morphology, that is reducing the sizes of the grains to nanoscale, the coupling between the two corresponding order parameters can be affected. As shown in a series of experiments on magnetic properties of nanosized manganites,[13,14,45,46] with decreasing the particle size from 2000 to 20–40 nm, the AFM order in the particles is suppressed leading to the weakening (in $La_{0.25}Ca_{0.75}MnO_3$) or complete disappearance (in $Pr_{0.5}Ca_{0.5}MnO_3$) of the charge order.

II. EXPERIMENT

Polycrystalline samples of $La_{1-x}Ca_xMnO_3$ were prepared according to the procedures described in Ref. 13. With the sol-gel method, the stoichiometric amounts of La_2O_3, $CaCO_3$, and 50% $Mn(NO_3)_2$ solution were taken as starting materials. La_2O_3 and $CaCO_3$ were converted into metal nitrates by adding nitric acid. These metal nitrates and excessive ethylene diamine tetraacetic acid (EDTA) were dissolved in distilled water to obtain a clear solution with a initial molar ratio of La:Ca:Mn=1:3:4. The pH of solution was adjusted to 6–7 by adding ethylenediamine and then an appropriate amount of ethylene glycol (EG) was added. Subsequently the solution was heated with stirring to evaporate most of the solvent water. The resultant gel precursors were decomposed at about 300 °C to obtain black precursor powder, which then was separated into several parts and annealed at temperatures from 600 to 1280 °C to gain samples with different particle sizes. The average particle sizes were characterized by field emission scan microscopy (FE-SEM, JEOL, JSM-6700F) and x ray using Scherrer formula. The structure characterization of the samples was done by x-ray diffraction on a MacScience MAXP18AHF diffractometer using Cu $K\alpha$ radiation.

For the optical measurements, we prepared pellets of 10 mm diameter and thicknesses varying from approximately 0.1–0.6 mm using a press machine with 6 tons force. All pellets had the same density. Optical measurements were performed on two spectrometers. In the THz range a coherent-source spectrometer (with backward-wave oscillators as radiation sources) was utilized, which allows for direct measurements of the complex conductivity $\sigma^*(\nu)$ or complex permittivity $\epsilon^*(\nu)$ at frequencies from $\nu=1$ cm^{-1} up to $\nu=50$ cm^{-1} and in the temperature interval from 2 up to 300 K. In a quasioptical arrangement of a Mach-Zehnder interferometer the complex transmission coefficients (amplitude and phase) of a plane-parallel samples are measured. Using standard Fresnel expressions for optics of layered structures,[37,47] any pair of optical parameters (complex conductivity, permittivity, refractive index, etc.) of the sample material is directly determined. All steps are described in details in Refs. 48–50. We can rule out any nonlinear effects in the interaction of the monochromatic THz radiation of a backward-wave oscillator with the samples that could influence the response functions. First, the intensity of the radiation (maximum of several milliwatts) is too small to heat up our samples mounted of a metal aperture that serves as an effective heat sink. The absence of radiation heating during the measurements on the THz spectrometer has been verified in many experiments, including measurements of very thin superconducting films when no effect on the transition temperature has been detected (see, for example, Refs. 51 and 52). Second, during the frequency scan the output intensity of the backward-wave oscillator changes by orders of magnitude; thus any nonlinearity would immediately appear in the spectra which, however, are always smooth. On the same pellets of $La_{1-x}Ca_xMnO_3$ also the far-infrared reflectivity was measured up to a frequency 700 cm^{-1} using a Fourier-transform IR (FTIR) spectrometer Bruker IFS 113 V. Combining these data with the THz reflectivity, measured or calculated from directly determined $\sigma(\nu)$ and $\epsilon'(\nu)$, and performing the Kramers-Kronig analysis allowed us to obtain spectra of real part of conductivity, $\sigma(\nu)$, and real part of permittivity, $\epsilon'(\nu)$, in a wide frequency interval from 4 up to 700 cm^{-1} (corresponding quantum energies from 0.4 to 90 meV).

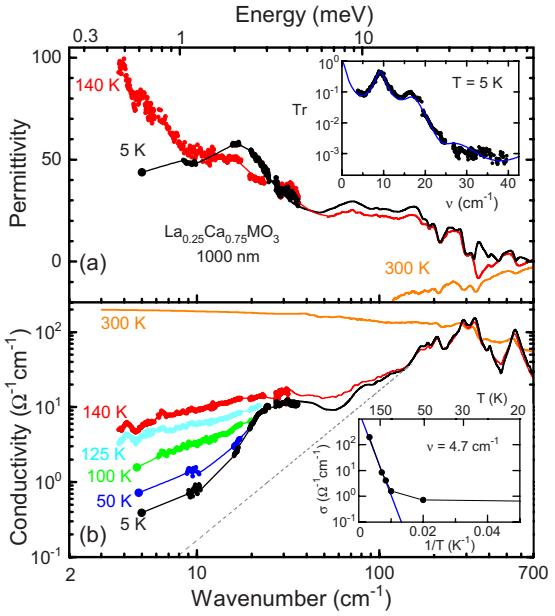

FIG. 1. (Color online) (a) Real part of dielectric permittivity of $La_{0.25}Ca_{0.75}MnO_3$ sample made of grains with 1000 nm diameter, as a function of frequency at temperatures $T=300$, 140, and 5 K. The symbols correspond to data directly obtained by a Mach-Zehnder interferometer; the solid and dashed lines result from reflectivity measurements via Kramers-Kronig analysis. (b) Optical conductivity plotted as a function of frequency for various temperatures as indicated. Again, the symbols correspond to data directly obtained by a Mach-Zehnder interferometer, solid and dashed lines are calculated from reflectivity measurements; the lines below 40 cm^{-1} are guides to the eye. The thin dotted line represents the ν^2 behavior of the conductivity indicating the low-frequency tail of the lowest infrared phonon. In the inset of panel (a) the transmission through a 0.076 mm thick plane-parallel pellet is shown (dots), measured at $T=5$ K. The solid line is obtained by a fit employing the Fresnel's expressions for a plane-parallel slab. The inset in panel (b) demonstrates in an Arrhenius plot the activated behavior of the low-frequency ($\nu=4.7$ cm^{-1}) conductivity with an activation energy 0.13 eV (straight blue line).

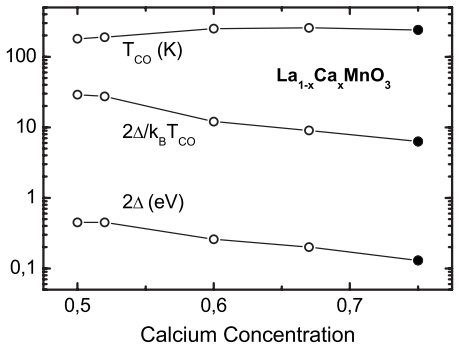

FIG. 2. Dependence of the charge-ordering temperature T_{CO}, the energy gap 2Δ, and of the ratio $2\Delta/T_{CO}$ of $La_{1-x}Ca_xMnO_3$ on calcium concentration x. The data given by open circles are obtained from infrared conductivity spectra from Ref. 42. The solid dots correspond to the values obtained in the present work based on the activated temperature behavior of the low-frequency ($\nu=4.7$ cm^{-1}) conductivity of polycrystalline $La_{0.25}Ca_{0.75}MnO_3$ with grains of 1 μm diameter.

III. EXPERIMENTAL RESULTS AND ANALYSIS

A. Bulk polycrystalline $La_{0.25}Ca_{0.75}MnO_3$

Figure 1 exhibits broadband permittivity and conductivity spectra of $La_{0.25}Ca_{0.75}MnO_3$ pellets with grains of 1 μm size. Our data obtained above $\nu\approx100$ cm^{-1} are similar to the IR spectra of polycrystalline samples of the same composition presented by Nucara *et al.*;[33] the phonon features are coinciding and there is only a small difference in absolute values of conductivity caused by different samples preparation procedures. This enables us to consider the electrodynamic properties of these samples as those of bulk polycrystalline material. From Fig. 1 it is seen that above the charge-ordering temperature $T_{CO}\approx240$ K the spectra of $La_{0.25}Ca_{0.75}MnO_3$ are typically metallic:[37,53] the conductivity $\sigma(\nu)$ is almost frequency independent, below 30 cm^{-1}, and decreases for higher frequencies; the permittivity $\epsilon'(\nu)$ is negative at small ν and increases toward high frequencies. Above 200 cm^{-1} phonon features are incompletely screened by itinerant carriers and are observed in the spectra $\sigma(\nu)$ and $\epsilon'(\nu)$.

When the sample is cooled below T_{CO}, the conductivity and permittivity spectra change their character qualitatively, from metallic to dielectriclike. Also the values of $\sigma(\nu)$ and $\epsilon'(\nu)$ change drastically, especially at the lowest frequencies of few wave numbers. For $T=5$ K, the conductivity drops by more than an order of magnitude and the permittivity increases from negative values (at 300 K) up to large positive values. As demonstrated in the inset of Fig. 1(b), in the range $T_N\approx140$ K$<T<T_{CO}\approx240$ K the conductivity is thermally activated $\sigma_T\propto\exp\{-E_{act}/k_BT\}$ with an activation energy $E_{act}=0.13$ eV, indicating an energy gap (pseudogap for $T>T_{CO}$) in the density of states. Corresponding gap features at this energy scale are seen in the infrared conductivity spectra of a series of manganites in the charge and/or orbitally ordered states,[41,42,54] Kim *et al.*[42] report a decrease in the gap values 2Δ and of the ratio $2\Delta/T_{CO}$ on calcium content x for $La_{1-x}Ca_xMnO_3$ ($0.48>x>0.67$). Our vales of $2\Delta=E_{act}$ and $2\Delta/T_{CO}$ for $x=0.75$ are in accord with this tendency (Fig. 2).

Below T_{CO}, the Drude-type metallic dispersion seen in the $\sigma(\nu)$ and $\epsilon'(\nu)$ spectra changes to the relaxational-like behavior,[55] the permittivity increases and the conductivity decreases toward low frequencies. To estimate the strength of the relaxation $\Delta\epsilon_D$, we fit the corresponding dispersion by the Debye expression for the complex permittivity,[55]

$$\epsilon_D^*(\nu)=\frac{\Delta\epsilon_D}{1-i\omega\tau_D}, \quad (1)$$

where $\omega=2\pi c\nu$ is circular frequency and $\tau_D=1/2\pi c\gamma_D$ is the relaxation time and c is the speed of light. We find that the strength of the relaxation $\Delta\epsilon_D$ weakens significantly upon cooling. Along with that, an absorption band appears in the range of 20–40 cm^{-1}. It starts to be reliably detected in the AFM phase, at $T<T_N=140$ K, getting most pronounced at the lowest temperatures and bearing the character of a resonance absorption, according to the "oscillating" dispersion of permittivity [for damping not exceeding the resonance fre-

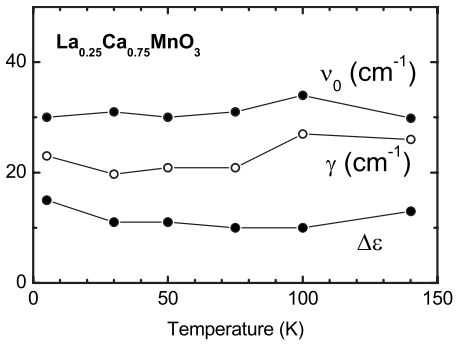

FIG. 3. Temperature dependence of the parameters of the absorption band observed in $La_{1-x}Ca_xMnO_3$ in the spectral range from 20 to 40 cm^{-1}: resonance frequency ν_0, damping constant γ, and dielectric strength $\Delta\epsilon$.

quency, see expression (2) below].[37] A close inspection reveals that the band consists of two resonances (absorption lines) located at frequencies around 25 and 40 cm^{-1}. Note, our spectra do not exhibit any resonance absorptions below 10 cm^{-1}, as reported in Ref. 33. This is also demonstrated in Fig. 1 and in the inset of panel (a) where the transmission coefficient is presented of a pellet 0.076 mm thick: here the low transmissivity of a pellet above 20 cm^{-1} is caused by absorption bands just discussed and the oscillating behavior at lower frequencies is connected to an interference (multireflection, Fabry-Perrot effect) of the radiation within a plane-parallel transparent layer of the sample.[37,47]

We fit the resonance dispersions seen at 20–40 cm^{-1} using the Lorentzian expression for complex conductivity,

$$\sigma^*(\nu) = \frac{0.5\Delta\epsilon\nu_0^2\nu}{\nu\gamma + i(\nu_0^2 - \nu^2)}, \tag{2}$$

where $\Delta\epsilon$ is the dielectric contribution (strength), ν_0 is the resonance frequency, and γ is the damping. The quality of our samples (pellets pressed of a powder) does not allow precise determination of all parameters, $\Delta\epsilon$, ν_0, and γ, of the two modes separately. We are able, however, to evaluate their resonance frequencies, 25 ± 3 cm^{-1} and 38 ± 3 cm^{-1}, and to find that they are practically temperature independent down to $T=5$ K. Most likely, also the strengths and the damping constants of the these modes are temperature independent; this is demonstrated in Fig. 3, where we show the temperature dependences of the dielectric strength, resonance frequency, and damping which would have the absorption band if considered as a single mode.

B. Nanosized $La_{0.25}Ca_{0.75}MnO_3$

After the analysis of the results for bulk material, we now move to the dependence of the electrodynamic properties on the grain size. In Fig. 4 we show how the broadband spectra of conductivity and permittivity of $La_{0.25}Ca_{0.75}MnO_3$ evolute when the grain size changes, from 1000 to 40 nm. In comparison with the bulk material, described in the previous section (Fig. 1), the dielectric response of samples with grain sizes 200 nm and smaller reveals significant quantitative and qualitative transformations, especially at the low-frequency side. At room temperature, in the paramagnetic state above

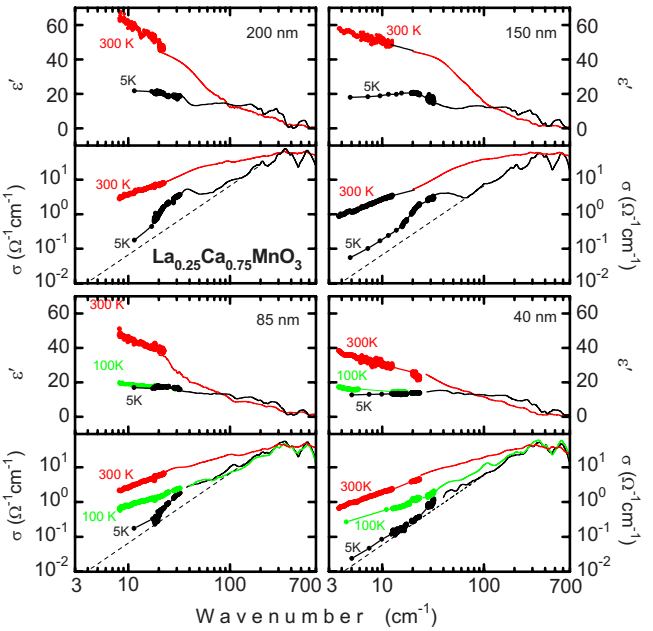

FIG. 4. (Color online) Spectra of the dielectric permittivity $\epsilon'(\nu)$ and conductivity $\sigma(\nu)$ of $La_{0.25}Ca_{0.75}MnO_3$ sample with various grain sizes, measured at different temperatures $T=300$, 100, and 5 K, as indicated. Upper left frame: 200 nm, upper right frame 150 nm, lower left frame 85 nm, and lower right frame 40 nm. The dashed straight lines represent the ν^2 behavior of the conductivity, which would correspond to the low-frequency tail of the lowest-frequency infrared phonon.

T_{CO}, not only the values of conductivity and permittivity of these samples differ notably from those of the bulk sample, but also the type of the dispersion of the $\sigma(\nu)$ and $\epsilon'(\nu)$ spectra has changed. Instead of a metallic Drude-type behavior, a typical relaxational dispersion[55] is observed in these spectra: a growth of $\sigma(\nu)$ and a decrease in $\epsilon'(\nu)$ toward high frequencies. Upon cooling down, similar to the bulk material, the strength of the relaxation $\Delta\epsilon_D$ decreases for all samples. Their granular structure has also crucial influence on the absorption band observed at frequencies 20–40 cm^{-1}: reducing the grain size, the band gradually disappears, as is demonstrated by Fig. 5, where the lowest temperature (5 K) spectra of permittivity and conductivity of 1000, 150, and 40 nm samples are summarized.

Besides the band around 20–40 cm^{-1}, a less intense and broad absorption band is quite reliably observed in the $\sigma(\nu)$ and $\epsilon'(\nu)$ spectra at higher frequencies 60–100 cm^{-1}. Comparing Figs. 1 and 4, it becomes obvious that this band is pronounced in the AFM phase but looses its intensity in the samples with smaller grains.

To see how the low-frequency features, the lowest-frequency relaxation and the resonancelike absorption band at 20–40 cm^{-1}, depend on the grain size of the samples, in Figs. 6(a) and 6(b) we plot the dependencies on the grain size of correspondent strengths, $\Delta\epsilon_D$ and $\Delta\epsilon$ [obtained from Eqs. (1) and (2)]. It is seen that the relaxation and the resonance absorption are loosing their weight for samples with granularity below 1000 nm, the strongest changes happening between 300 and 1000 nm. It is interesting that in the same range of grain sizes also the activation energy strongly de-

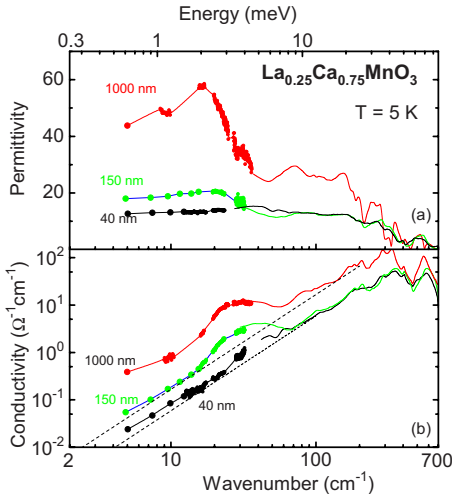

FIG. 5. (Color online) Comparison of the dielectric permittivity $\epsilon'(\nu)$ and conductivity $\sigma(\nu)$ of $La_{0.25}Ca_{0.75}MnO_3$ sample consisting of different grain sizes measured at liquid-helium temperature. The curves are derived from reflectivity measurements, the dots are directly measured using the Mach-Zehnder interferometer. Lines below 40 cm^{-1} are guides to the eye. Dashed straight lines represent the ν^2 behavior of the conductivity that would correspond to the low-frequency tail of the lowest-frequency infrared phonon.

creases [Fig. 6(c)] that governs the temperature variation in the lowest frequency (about 10 cm^{-1}) conductivity [Fig. 1(b)]. Grain-size effects influence also the charge-ordering temperature, as determined by the magnetization curves,[13] T_{CO} is significantly reduced for grains of size less than 100–200 nm, as depicted in Fig. 6(d).

In Figs. 6(e), 6(f), and 7 we plot the grain size and the temperature dependences of the "background" dielectric response of $La_{0.25}Ca_{0.75}MnO_3$, i.e., the temperature dependences of ϵ' and σ at frequencies below the resonance features. Variations in ϵ' and σ with the grain size are most pronounced above T_{CO}, indicating that they are caused mainly by delocalized charge carriers dominant at room temperature. Again, the largest variation takes place between 300 and 1000 nm. For all samples the CO phase transition is clearly pronounced in both, $\sigma(T)$ and $\epsilon'(T)$ (for 1000 nm sample only data below 140 K are available). For the 200 nm specimen the dielectric permittivity starts to decrease at T_{CO} and saturates in the AFM phase. For samples with smaller grains the CO-transition temperature shifts down and the transition region becomes broader, similar to what is seen in magnetic measurements.[13] The same behavior is observed in the temperature dependence of the conductivity: $\sigma(T)$ changes much stronger than the values of permittivity, decreasing by more than an order of magnitude while cooling from 300 to 5 K. Interestingly, while the permittivity changes only for temperatures between T_{CO} and T_N and stays constant below T_N, the conductivity exhibits a strong temperature dependence also in the AFM phase. For comparison, in Fig. 7 the temperature dependence of the dc conductivity is presented for polycrystalline bulk sample of the same composition $La_{0.25}Ca_{0.75}MnO_3$, data taken from Ref. 56. Above T_{CO} the dc conductivity is higher and below T_{CO} smaller than the ac conductivity which can be attributed to an intrinsic or

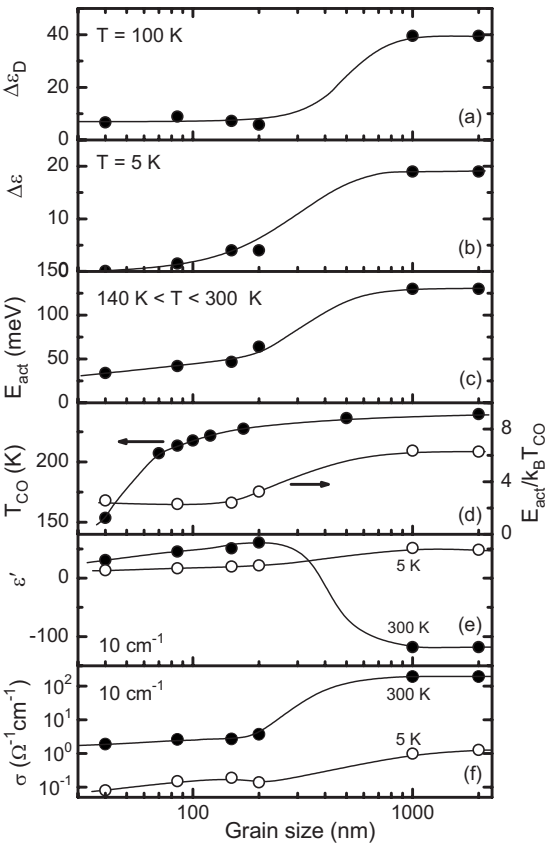

FIG. 6. Grain-size dependences of various characteristic parameters of $La_{0.25}Ca_{0.75}MnO_3$. (a) Dielectric strength $\Delta\epsilon_D$ of the relaxation seen at the lowest frequencies in the permittivity and conductivity spectra at $T=100$ K. (b) Dielectric strength $\Delta\epsilon$ of the absorption band in the range 20–40 cm^{-1} at $T=5$ K. (c) Activation energy E_{act}, describing the exponential temperature behavior of the low-frequency (5–10 cm^{-1}) conductivity $\sigma(T) \propto \exp\{-E_{act}/k_BT\}$ in the range $140<T<300$ K. (d) Charge-ordering temperature T_{CO} (left axis), defined from measurements of the magnetization and lattice parameters (Ref. 13), and "strength" of charge-ordering interaction E_{act}/k_BT_{CO} (right axis). (e) Low-frequency (10 cm^{-1}) permittivity for $T=5$ and 300 K, and (f) optical conductivity at fixed frequency $\nu=10$ cm^{-1}. The lines are guides to the eye.

extrinsic localization of charges and hopping conduction, as discussed in the next section.

IV. DISCUSSION

A. Bulk polycrystalline $La_{0.25}Ca_{0.75}MnO_3$

The room-temperature spectra of the optical conductivity and permittivity displayed in Fig. 1 are typical for materials containing free charge carriers with phonon features superimposed in the infrared range above 100–200 cm^{-1}. This picture changes with decreasing temperature. The activated thermal behavior of the lowest-frequency conductivity [inset in Fig. 1(b)] is a clear manifestation of an energy gap (or pseudogap for $T>T_{CO}$) with the value $2\Delta=E_{act}=0.13$ eV (corresponding frequency is approximately 1000 cm^{-1}) present in the density of states at temperatures 100–300 K.

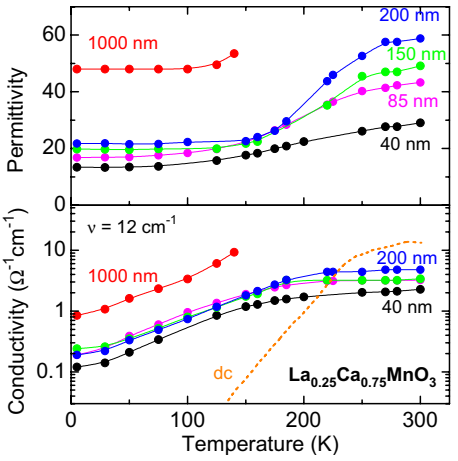

FIG. 7. (Color online) Temperature dependence of the low-frequency (ν=12 cm^{-1}) permittivity and conductivity of $La_{0.25}Ca_{0.75}MnO_3$ samples with different grain sizes as indicated. For the 1000 nm sample, data are available only below T=140 K. The solid lines are guides to the eye. The dashed line shows the temperature dependence of the dc conductivity of polycrystalline $La_{0.25}Ca_{0.75}MnO_3$ taken from Ref. 56.

This gap feature is also detected as a thresholdlike increase around 1000 cm^{-1} in the infrared conductivity spectra of manganites of different compositions, including $La_{0.25}Ca_{0.75}MnO_3$.[33,40–42,57] It is generally accepted that these gaps or pseudogaps are caused by the long-range charge order below the critical temperature T_{CO} or by correspondent order-parameter fluctuations above T_{CO}.

We argue that optical experiments do not provide any evidence of a CDW state in manganites. First of all, the optical gap values are too large compared to what is expected from the mean-field value $2\Delta_{CDW}/k_BT_{CDW} \approx 3.5$. For LCMO these values range from $2\Delta/k_BT_{CO} \approx 30$ for x=0.5 (Ref. 42) to $2\Delta/k_BT_{CO} \approx 6$ for x=0.75 (present data). Also the low-energy band around 20–40 cm^{-1} cannot be assigned to a pinned CDW phason mode since: (i) this band consists of two peaks while the CDW phason excitation is represented by a single mode.[27] (ii) Usually the CDW mode is significantly broadened and overdamped; this would also be expected in manganites with "dirty Peierls transition."[31,58] In our spectra, however, the band is clearly underdamped, as seen in the permittivity spectra plotted in Fig. 1(a). (iii) The dielectric strength $\Delta\epsilon$ of the band is temperature independent, contrary to what is observed for CDW in low-dimensional conductors.[27] We propose a more trivial origin of the absorption features observed in our optical investigations. We suggest that they originate from acoustic phonons activated by the folding of the Brillouin zone caused by a superstructure which appears in the crystal lattice of manganites in the CO and AFM ordered states. The x-ray investigations of $La_{0.25}Ca_{0.75}MnO_3$ (Ref. 29) demonstrated that the high-temperature phase has the orthorhombic unit cell with a space group *Pnma*. It was shown also that additional diffraction peaks appear below the charge-ordering temperature T_{CO}=240 K, signaling the development of a superlattice: the unit cell multiplies by a factor of 4 along the a axis. Below we present simple symmetry-related considerations that confirm our suggestion. The $4a$ superstructure is related to a new phase with symmetry of the space group $P2_1/m(C_{2h}^2)$. Consequently, the phase transition at the temperature T_{CO} should be described by the order parameter that is transformed with the wave vector $q_x=\pi/(4a)$ of the Brillouin zone of the high-temperature phase according to the irreducible representation of the space group *Pnma*. There are four one-dimensional irreducible representations corresponding to the point symmetry group C_{2v} of the wave vector $q_x=\pi/(4a)$ in the *Pnma* phase. Since the vectors $\pm q_x$ of the points within the Brillouin zone are not equivalent, the full representations are two dimensional; we can denote them as Σ_i (i=1–4). Each of the order parameters (Σ_i) induces three low-symmetry phases. A simple group-theoretical analysis shows that the phase with the $P2_1/m(C_{2h}^2)$ symmetry is only realized during a condensation order parameter (Σ_1). If we know the order parameter that induces the $P2_1/m(C_{2h}^2)$ phase, we can perform correlations of irreducible representations of the groups *Pnma* and $P2_1/m$. Let us first consider the transformation of the acoustic modes in $La_{0.25}Ca_{0.75}MnO_3$. In an orthorhombic phase their symmetries are described by the following representations: two transverse-acoustic modes have the symmetry $\Sigma_3(\mathrm{TA},z)$ and $\Sigma_4(\mathrm{TA},y)$, and the longitudinal-acoustic mode has the symmetry $\Sigma_1(\mathrm{LA},x)$. In parentheses the character of the mode and its polarization are shown. As a result of the $Pnma \leftrightarrow P2_1/m$ structural phase transition, the phonons with the wave vector $q_x=\pi/(4a)$ are folded to the Brillouin-zone center of the monoclinic phase and are split into two phonons symmetric and antisymmetric, relative to the center of inversion; in other words, they are split into the (g,u) pairs. The gerade modes (A_g and B_g), which are symmetric relative to the inversion center, become optically Raman-active phonons, while the ungerade modes (A_u and B_u) are antisymmetric relative to the inversion center, they form polarization waves and become IR active. In the case of $La_{0.25}Ca_{0.75}MnO_3$ the optical activity of these modes is promoted by a dipole moment produced by spatial charge disproportionation which includes all ions of the new unit cell together with the valence difference on manganese ions. Note that the Brillouin-zone folding accompanying the $Pnma \leftrightarrow P2_1/m$ phase transition also reflects the phonons from the X point (i.e., from the Brillouin-zone boundary of the phase *Pnma*) onto the Γ point of the $P2_1/m$ phase Brillouin zone.

The described transformation, corresponding to the observed evolution of the low-frequency spectra of $La_{0.25}Ca_{0.75}MnO_3$, is depicted in Fig. 8. The figure should be considered only semiquantitatively since the data of single-crystalline solid solutions of this composition are presently not available. Though, there are calculations of the phonon branches for $LaMnO_3$ (Ref. 59) that are expected to be close to the results of Fig. 8. In constructing Fig. 8(c) we took into account also that in the paraphase of $La_{0.25}Ca_{0.75}MnO_3$ the phonon resonances appear at frequencies 120–130 cm^{-1}. From that figure it is obvious that the absorption band we observe in $La_{0.25}Ca_{0.75}MnO_3$ around 30–40 cm^{-1} corresponds to the modes with the wave vector $q_x=\pi/(4a)$ while the broad set of superimposed bands at frequencies below 100 cm^{-1} has to be associated with the Brillouin-zone

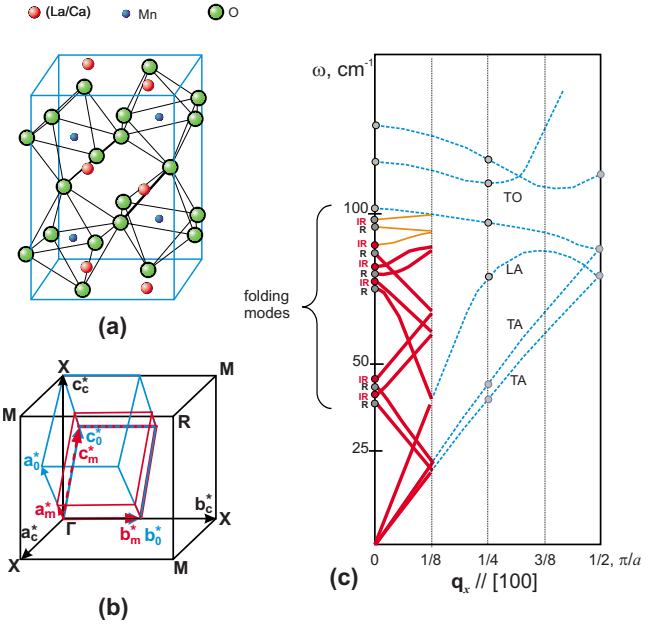

FIG. 8. (Color online) (a) Unit cell of $(La,Ca)MnO_3$ in the orthorhombic *Pnma* phase. (b) Transformation of the Brillouin zone of a cubic perovskitelike unit cell at the $Pm3m \leftrightarrow Pnma \leftrightarrow P2_1/m$ phase transitions, leading to supercell of $4a$. (c) Qualitative scheme demonstrating the folding of the modes at the $Pnma \leftrightarrow P2_1/m$ phase transition. The acoustic phonons with $q_x=\pi/(4a)$ and $q_x=\pi/(2a)$ (gray dots) in *Pnma* structure are folded to the center of the monoclinic zone and become Raman-active (open dots) and infrared-active (filled dots) optic modes. The band in the frequency range around 20–40 cm^{-1} is formed by modes with wave vector $q_x=\pi/(4a)$ and the band around 100 cm^{-1} is formed by modes with wave vector $q_x=\pi/(2a)$ from the Brillouin-zone boundary. Certain contributions to the low-frequency part of the band around 100 cm^{-1} can come from the phonons with the wave vector $q_x=\pi/(3a)$ (phase with supercell $3a$) (Ref. 29).

boundary modes of wave vectors $q_x=\pi/(2a)$. It is apparent, that the blurred character of the two groups of folded phonons is a consequence of a polycrystalline nature of the samples with all three crystallographic directions contributing to the optical response. Also multiple phases might be present below T_N, such as a phase with the $3a$ superlattice.[29]

Finally, we want to note that the appearance of the broadband at 30–40 cm^{-1} only in the AFM phase and not right below the CO transition temperature correlates well with the temperature evolution of the weight fraction of the new $4a$ phase which starts to increase below T_{CO} and reaches its full strength only below T_N.[29] We definitely rule out the magnetic origin of the band because the antiferromagnetic-resonance modes are of much smaller strengths (10^{-2} or less) compared to $\Delta\epsilon \approx 20$ in our case. In addition, their resonance frequencies are strongly temperature dependent, in contrast to our observations presented in Fig. 3 (see, for example, Ref. 60).

B. Nanosized $La_{0.25}Ca_{0.75}MnO_3$

As seen from Figs. 4, 5, and 6(b), the phonon bands that appear in the AFM phase of $La_{0.25}Ca_{0.75}MnO_3$ due to Brillouin-zone folding weaken gradually as the sample grain size becomes smaller, indicating suppression of the $4a$ superlattice in small grains. Considering this superlattice as one of the essential constituents of the charge-ordered phase,[23] we thus conclude from our optical measurements that the CO correlations get weaker in small grains, which is consistent with the results of magnetic measurements.[13,14] The partial suppression of the charge order is also illustrated by the decreasing CO gap $2\Delta=E_{act}$ and decrease in the CO correlations strength $2\Delta/T_{CO}$ [Figs. 6(c) and 6(d)]. When the particle size gets below 200–300 nm, both quantities decrease significantly: they do not vanish completely with a sizable values remaining down to the smallest grains of 40 nm. At the same time the dielectric strength of the folded phonon modes and of the corresponding $4a$ superlattice almost completely disappear for the 40 nm particles at $T=5$ K, suggesting that the dynamics of the crystal lattice does not play a crucial role in the formation of the CO state. These our observations indicate that these structural effects are only some by-products of a complex interplay between charge, spin, and orbital interactions. This important conclusion is strongly supported by the fact that the $4a$ superstructure and corresponding folded phonon modes are fully stabilized not right at T_{CO} but only by cooling well into the AFM phase.[23] Supporting evidence could be obtained from a study of the folded phonons and their evolution in bulk and in nanograined manganites consisting of other concentrations of alkali element since a variation in x drastically alters the stability of and the balance between the different interactions. For instance, the small FM surface component in $La_{0.25}Ca_{0.75}MnO_3$ is a consequence of a stable AFM state,[44,56,61] in contrast to the $La_{0.5}Ca_{0.5}MnO_3$ compound where both CO and AFM phases are fully suppressed in nanoparticles of 10–20 nm size.[46] The charge gap 2Δ and the interaction strength measured by $2\Delta/T_{CO}$ systematically decrease from $2\Delta=0.45$ eV and $2\Delta/k_BT_{CO}=30$ at $x=0.5$ to $2\Delta=0.2$ eV and $2\Delta/k_BT_{CO}=9$ for $x=0.67$ (Ref. 42) and further to $2\Delta=0.13$ eV and $2\Delta/k_BT_{CO}=6.3$ for the composition $x=0.75$ (present data). According to the results of Kim *et al.*,[42] we predict a pronounced dependence of frequency positions of the folded phonon modes on the variation in the alkali-metal concentration x because the lattice modulation wave vector q^* is unambiguously connected to the composition, $q^*=a^*(1-x)$ (a^* is the reciprocal-lattice vector along a).[23,62,63]

As for the mechanism of suppression of the superlattice in nanograins, it is unlikely that it is connected with a commensurability of its period $4a \approx 2$ nm and the minimal grain size of 40 nm is too large. Alternatively Sarkar *et al.*[14,46] suggested that the tension on the grain surface produces considerable hydrostatic pressure in the bulk that hinders the lattice parameter to grow in the CO or AFM states and thus stabilizes the high-temperature paramagnetic phase. Since the main changes of charge and magnetic characteristics in $La_{0.25}Ca_{0.75}MnO_3$ and $La_{0.5}Ca_{0.5}MnO_3$ (Ref. 46) take place in the same particles dimension, we suppose that in this range the hydrostatic pressure reaches a certain critical value (several gigapascals), comparable to the intrinsic forces that drive the structural transformations.

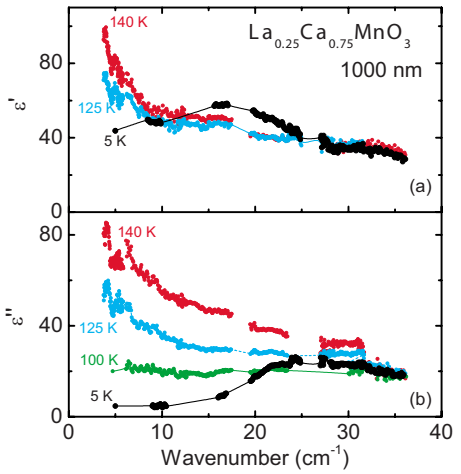

FIG. 9. (Color online) Low-frequency spectra of (a) real and (b) imaginary parts of dielectric permittivity, ϵ' and ϵ'', of polycrystalline sample $La_{0.25}Ca_{0.75}MnO_3$ (grain size of 1000 nm) measured in Mach-Zehnder geometry at different temperatures as indicated. The lines are guides to the eye.

C. Low-frequency relaxation

Finally let us consider the relaxational behavior of permittivity and conductivity, observed at our lowest frequencies, $\nu \leq 10$ cm^{-1}, as shown in Fig. 1 and in more details in Fig. 9. As seen in the Fig. 9, no maximum is recorded in the spectrum of imaginary part of the permittivity, $\varepsilon'' = 2\sigma/\nu$, as would be expected in case of a simple Debye relaxation with the maximum in $\varepsilon''(\nu)$ at a specific frequency of the relaxation process $\gamma = 1/(2\pi c\tau_D)$ (τ_D is the relaxation time).[55] This implies that either the characteristic frequency γ_D of relaxation is located below the frequency window accessible by our experiments or a distribution of relaxation times (frequencies) exists that leads to a significant broadening of the spectral response. The relaxation is most pronounced at the elevated temperatures; it becomes weaker as the temperature is lowered and the free carrier concentration decreases, according to the ac and dc conductivity (Fig. 7). It is obvious from our data that the origin of the relaxation is intimately related to the itinerant charge carriers. However, its connection to simple geometrical localization of carriers within the grains—which may be considered as "boxes"—can be ruled out; it would cause a dispersion similar to the one expected in the "metallic strands model" of Rice and Bernasconi[64] that does not correspond to our observations. In the present case of a grain size $d = 1$ μm and a Fermi velocity $v_F = 10^9$ cm/s (Ref. 28) the characteristic relaxation frequency is estimated at $\nu_{rel} \approx v_F/d = 10^{13}$ Hz ≈ 300 cm^{-1}, which falls well above the frequency range where we observe the corresponding dispersion of $\varepsilon'(\nu)$ and $\sigma(\nu)$. Also for smaller grains, the characteristic frequency would move to higher frequencies, in contrast to our observations. Alternatively, one may suggest that the carriers are localized by grain boundaries producing a Maxwell-Wagner-type relaxation in the spectra. However, for smaller grains the ratio surface/volume increases, which would lead to an enhanced relaxation strength ($\Delta\epsilon_D$); opposite to what is observed in our measurements, as demonstrated in Fig. 6(a).

We therefore conclude that the relaxational dispersion observed in the low-frequency permittivity and conductivity spectra of $La_{0.25}Ca_{0.75}MnO_3$ is intrinsic and connected to the charge-ordering process. This dielectric response resembles the "order-disorder" phase transitions, found in ferroelectrics, for instance, or in ferroelectrics and dipole glass (relaxors),[65] where the potential energy of the system is characterized by two or more minima.[66] At high temperatures, the minima are randomly occupied due to thermal disorder. Below the transition temperature, the system components drop into the deepest minima, and the order parameter (polarization in case of ferroelectrics, for example) acquires a nonzero value. The dynamics of such phase transitions are commonly described by a relaxation behavior of a certain response function with a relaxation time or distribution of relaxation times revealing definite temperature dependences.[65] The phase transition to the charge-ordered state in manganites might be of this kind: i.e., an order-disorder transition where the itinerant charges experience the periodical array of localizing sites on manganese or oxygen positions. It is also possible that the relaxational dispersion in the spectra is due to a phase transition to the ferroelectric state. Efremov *et al.*[67] reported that in manganites the interplay between charge and magnetism can lead to ferroelectricity with the dipole moment aligned along the diagonal between the *a* and *b* axes. It is caused by a coupling between the charge and magnetic density waves on the bonds. Although the correspondent polarization would be much smaller than that in "classical" ferroelectrics such as $BaTiO_3$, this novel type of ferroelectricity deserves experimental verification. Hence we suggest detailed measurements of the dielectric spectra of manganites of various compositions, in particular, looking at the low-frequency relaxation spectra in the THz and microwave frequency ranges.

V. CONCLUSION

By using the coherent-source THz spectroscopy, combined with FTIR measurements, we have investigated the conductivity and dielectric permittivity spectra of $La_{0.25}Ca_{0.75}MnO_3$ at frequencies from 4 to 700 cm^{-1}. In bulk polycrystalline samples with grains of several micrometers, the low-frequency conductivity is thermally activated with an energy gap $2\Delta = 0.13$ eV in the density of states at temperatures $T > 140$ K, that is seen as a gap below, or a pseudogap above the charge-ordering temperature $T_{CO} \approx 240$ K. In the antiferromagnetically ordered phase at $T < 140$ K, a resonancelike absorption band appears in the spectra around 20–40 cm^{-1}. We assign it to acoustical phonons, which gain optical activity when folded to the Brillouin-zone center due to a structural phase transition connected with an appearance of a fourfold $4a$ superstructure in the crystallographic *a* direction. In contrast to previous claims by other groups, we did not observe any optical excitation at energies down to 0.4 meV that could be associated with the collective response of the charge-ordered electronic condensate. In order to study the nanosize effects, we studied

the response of samples with grain diameters ranging from several micrometers (considered as polycrystalline bulk samples) down to 40 nm. With decreasing grain size, the $4a$ superlattice and hence the absorption band are gradually suppressed while the charge and the antiferromagnetic orders survive, indicating a weak coupling of the correspondent order parameters to the crystal lattice. At the lowest frequencies $4-20$ cm^{-1} a strong relaxation in the conductivity and permittivity spectra is observed above 100 K in all samples. It may indicate an order-disorder character of the charge-order phase transition in this compound.

ACKNOWLEDGMENTS

We acknowledge helpful discussions with P. Arseev, P. Calvani, D. Efremov, N. Kovaleva, A. Mukhin, S. Tomić, and V. Travkin. T.Z. and D.W. thank the Alexander von Humboldt Foundation for their support. Funding from the Deutsche Forschungsgemeinschaft (DFG) and by the RAS Program for fundamental research "Strongly correlated electrons in solids and solid structures" and Russian Foundation for Basic Research (Project No. 08-02-00757a) is acknowledged.

[1] R. von Helmolt, J. Wecker, B. Holzapfel, L. Schultz, and K. Samwer, Phys. Rev. Lett. **71**, 2331 (1993).
[2] S. Jin, T. H. Tiefel, M. McCormack, R. A. Fastnacht, R. Ramesh, and L. H. Chen, Science **264**, 413 (1994).
[3] *Colossal Magnetoresistance, Charge Ordering and Related Properties of Manganese Oxides*, edited by C. N. R. Rao and B. Raveau (World Scientific, Singapore, 1998).
[4] *Colossal Magnetoresistance Oxides*, edited by Y. Tokura (Gordon and Breach, New York, 2000).
[5] E. Dagotto, T. Hotta, and A. Moreo, Phys. Rep. **344**, 1 (2001).
[6] H. Kuwahara, Y. Tomioka, A. Asamitsu, Y. Morimoto, and Y. Tokura, Science **270**, 961 (1995).
[7] A. Asamitsu, Y. Tomioka, H. Kuwahara, and Y. Tokura, Nature (London) **388**, 50 (1997).
[8] D. P. Kozlenko, Z. Jirak, I. N. Goncharenko, and B. N. Savenko, J. Phys.: Condens. Matter **16**, 5883 (2004).
[9] C. Cui and T. A. Tyson, Phys. Rev. B **70**, 094409 (2004).
[10] V. Kiryukhin, D. Casa, J. P. Hill, B. Keimer, A. Vigliante, Y. Tomioka, and Y. Tokura, Nature (London) **386**, 813 (1997).
[11] D. E. Cox, P. G. Radaelli, M. Marezio, and S.-W. Cheong, Phys. Rev. B **57**, 3305 (1998).
[12] T. Mori, K. Ogawa, K. Yoshida, K. Miyano, Y. Tomioka, and Y. Tokura, J. Phys. Soc. Jpn. **66**, 3570 (1997).
[13] T. Zhang, T. F. Zhou, T. Qian, and X. G. Li, Phys. Rev. B **76**, 174415 (2007).
[14] T. Zhang and M. Dressel, Phys. Rev. B **80**, 014435 (2009).
[15] S.-W. Cheong and H. Y. Hwang, *Colossal Magnetoresistance Oxides* (Ref. 4), p. 237.
[16] J. Goodenough, Phys. Rev. **100**, 564 (1955).
[17] S. Mori, C. H. Chen, and S.-W. Cheong, Nature (London) **392**, 473 (1998).
[18] C. H. Chen, S.-W. Cheong, and H. Y. Hwang, J. Appl. Phys. **81**, 4326 (1997).
[19] R. Wang, J. Gui, Y. Zhu, and A. R. Moodenbaugh, Phys. Rev. B **61**, 11946 (2000).
[20] P. G. Radaelli, D. E. Cox, L. Capogna, S.-W. Cheong, and M. Marezio, Phys. Rev. B **59**, 14440 (1999).
[21] J. Herrero-Martín, J. García, G. Subías, J. Blasco, and M. Concepción Sánchez, Phys. Rev. B **70**, 024408 (2004).
[22] M. Coey, Nature (London) **430**, 155 (2004).
[23] J. C. Loudon, S. Cox, A. J. Williams, J. P. Attfield, P. B. Littlewood, P. A. Midgley, and N. D. Mathur, Phys. Rev. Lett. **94**, 097202 (2005).
[24] S. Cox, E. Rosten, J. C. Chapman, S. Kos, M. J. Calderon, D. J. Kang, P. B. Littlewood, P. A. Midgley, and N. D. Mathur, Phys. Rev. B **73**, 132401 (2006).
[25] O. V. Ivanov and E. G. Maksimov, Solid State Commun. **76**, 1267 (1990).
[26] G. C. Milward, M. J. Calderón, and P. B. Littlewood, Nature (London) **433**, 607 (2005).
[27] G. Grüner, *Density Waves in Solids* (Addison-Wesley, Reading, 1994).
[28] Y.-G. Chuang, A. D. Gromko, D. S. Dessau, T. Kimura, and Y. Tokura, Science **292**, 1509 (2001).
[29] M. Pissas, I. Margiolaki, K. Prassides, and E. Suard, Phys. Rev. B **72**, 064426 (2005).
[30] A. Wahl, S. Mercone, A. Pautrat, M. Pollet, Ch. Simon, and D. Sedmidubsky, Phys. Rev. B **68**, 094429 (2003).
[31] S. Cox, J. Singleton, R. D. McDonald, A. Migliori, and P. B. Littlewood, Nature (London) **7**, 25 (2008).
[32] N. Kida and M. Tonouchi, Phys. Rev. B **66**, 024401 (2002).
[33] A. Nucara, P. Maselli, P. Calvani, R. Sopracase, M. Ortolani, G. Gruener, M. Cestelli Guidi, U. Schade, and J. Garcia, Phys. Rev. Lett. **101**, 066407 (2008).
[34] M. Dressel, N. Drichko, and S. Kaiser, Physica C (to be published).
[35] R. Schmidt, Phys. Rev. B **77**, 205101 (2008).
[36] B. Fisher, J. Genossar, L. Patlagan, and G. M. Reisner, J. Magn. Magn. Mater. (to be published).
[37] M. Dressel and G. Grüner, *Electrodynamics of Solids* (Cambridge University Press, Cambridge, 2002).
[38] S. V. Dordevic and D. N. Basov, Ann. Phys. **15**, 545 (2006).
[39] D. N. Basov, R. D. Averitt, D. van der Marel, M. Dressel, and K. Haule, Rev. Mod. Phys. (to be published).
[40] J. H. Jung, H. J. Lee, T. W. Noh, E. J. Choi, Y. Moritomo, Y. J. Wang, and X. Wei, Phys. Rev. B **62**, 481 (2000).
[41] Y. Okimoto, Y. Tomioka, Y. Onose, Y. Otsuka, and Y. Tokura, Phys. Rev. B **59**, 7401 (1999).
[42] K. H. Kim, S. Lee, T. W. Noh, and S.-W. Cheong, Phys. Rev. Lett. **88**, 167204 (2002).
[43] B. P. Gorshunov, A. Volkov, A. S. Prokhorov, I. E. Spektor, J. Akimitsu, M. Dressel, G. J. Nieuwenhuys, S. Tomic, and S. Uchida, Quantum Electron. **37**, 916 (2007).
[44] T. Qian, R. K. Zheng, T. Zhang, T. F. Zhou, W. B. Wu, and X. G. Li, Phys. Rev. B **72**, 024432 (2005).
[45] X. H. Huang, J. F. Ding, G. Q. Zhang, Y. Hou, Y. P. Yao, and X. G. Li, Phys. Rev. B **78**, 224408 (2008).
[46] T. Sarkar, B. Ghosh, A. K. Raychaudhuri, and T. Chatterji, Phys.

Rev. B **77**, 235112 (2008).
[47] M. Born and M. Wolf, *Principles of Optics*, 7th ed. (Cambridge University Press, Cambridge, 1999).
[48] G. Kozlov and A. Volkov, in *Millimeter and Submillimeter Wave Spectroscopy of Solids*, edited by G. Grüner (Springer, Berlin, 1998).
[49] B. P. Gorshunov, A. Volkov, I. E. Spektor, A. S. Prokhorov, A. A. Mukhin, M. Dressel, S. Uchida, and A. Loidl, Int. J. Infrared Millim. Waves **26**, 1217 (2005).
[50] B. P. Gorshunov, A. A. Volkov, A. S. Prokhorov, and I. E. Spektor, Phys. Solid State **50**, 2001 (2008).
[51] M. Dressel, N. Drichko, B. Gorshunov, and A. Pimenov, IEEE J. Sel. Top. Quantum Electron. **14**, 399 (2008).
[52] B. Gorshunov, D. Wu, A. A. Voronkov, P. Kallina, K. Iida, S. Haindl, F. Kurth, L. Schultz, B. Holzapfel, and M. Dressel, Phys. Rev. B **81**, 060509(R) (2010).
[53] A. V. Sokolov, *Optical Properties of Metals* (American Elsevier, New York, 1967).
[54] I. Kezsmarki, Y. Tomioka, S. Miyasaka, L. Demko, Y. Okimoto, and Y. Tokura, Phys. Rev. B **77**, 075117 (2008).
[55] A. K. Jonscher, *Dielectric Relaxation in Solids* (Chelsea Dielectric Press, London, 1983).
[56] X. G. Li, R. K. Zheng, G. Li, H. D. Zhou, R. X. Huang, J. Q. Xie, and Z. D. Wang, Europhys. Lett. **60**, 670 (2002).
[57] P. Calvani, G. De Marzi, P. Dore, S. Lupi, P. Maselli, F. D'Amore, S. Gagliardi, and S. W. Cheong, Phys. Rev. Lett. **81**, 4504 (1998).
[58] S. Cox, J. C. Lashley, E. Rosten, J. Singleton, A. J. Williams, and P. B. Littlewood, J. Phys.: Condens. Matter **19**, 192201 (2007).
[59] E. G. Rini, M. N. Rao, S. L. Chaplot, N. K. Gaur, and R. K. Singh, Phys. Rev. B **75**, 214301 (2007).
[60] D. Ivannikov, M. Biberacher, H.-A. Krug von Nidda, A. Pimenov, A. Loidl, A. A. Mukhin, and A. M. Balbashov, Phys. Rev. B **65**, 214422 (2002).
[61] X. G. Li, H. Chen, C. F. Zhu, H. D. Zhou, R. K. Zheng, and J. H. Zhang, Appl. Phys. Lett. **76**, 1173 (2000).
[62] L. Brey, Phys. Rev. Lett. **92**, 127202 (2004).
[63] S. Cox, J. C. Loudon, A. J. Williams, J. P. Attfield, J. Singleton, P. A. Midgley, and N. D. Mathur, Phys. Rev. B **78**, 035129 (2008).
[64] M. J. Rice and J. Bernasconi, J. Phys. F: Met. Phys. **3**, 55 (1973).
[65] R. Blink and B. Zeks, *Soft Modes in Ferroelectrics and Antiferroelectrics* (North-Holland, Amsterdam, 1974).
[66] N. F. Mott, *Metal-Insulator Transitions*, 2nd ed. (Taylor & Francis, Bristol, 1990); N. P. Mott and E. A. Davis, *Electronic Processes in Non-Crystalline Materials*, 2nd ed. (Clarendon Press, Oxford, 1979).
[67] D. Efremov, J. van den Brink, and D. Khomskii, Nature Mater. **3**, 853 (2004).